

# Heavy Daily Precipitation Events in the CMIP6 Worst-Case Scenario: Projected Twenty-First-Century Changes

ENRICO SCOCCIMARRO AND SILVIO GUALDI

*Fondazione Centro Euro-Mediterraneo sui Cambiamenti Climatici, Bologna, Italy*

(Manuscript received 13 December 2019, in final form 9 June 2020)

## ABSTRACT


Heavy precipitation is often the trigger for flooding and landslides, leading to significant societal and economic impacts, ranging from fatalities to damage to infrastructure to loss of crops and livestock. Therefore, it is critical that we have a better understanding of how it may be changing in the future. Based on model projections from phases 3 and 5 of the Coupled Model Intercomparison Project (CMIP3 and CMIP5), future daily precipitation is likely to increase in intensity. The main goal of this study is to examine possible improvements in the representation of intense and extreme precipitation by a new set of climate models contributing to phase 6 of CMIP effort (CMIP6) and to quantify its projected changes under the highest emissions scenario by the end of the current century [i.e., Shared Socioeconomic Pathway (SSP) SSP5-8.5]. Daily precipitation data from six CMIP6 models were analyzed that have a nominal horizontal grid spacing around 100 km and provide data for the highest emissions scenario SSP5-8.5. Two of the six CMIP6 models overestimate the extreme precipitation (defined as the 99th percentile of the precipitation distribution) in the tropics, leading to large biases in the right tail of the daily precipitation over the tropics. Consistent with the CMIP5 results, the CMIP6 models projected increased heavy daily precipitation and increased width of the right tail of the precipitation distribution associated with increased water vapor content.

## 1. Introduction

Changes in intense precipitation events are one major concern of climate change. Future climate projections from phases 3 and 5 of the Coupled Model Intercomparison Project [CMIP3 (Meehl et al. 2007) and CMIP5 (Meehl and Bony 2012; Taylor et al. 2012)] projects allowed the investigation of precipitation and other changes under different twenty-first-century emissions scenarios. Many studies have used climate simulations by both global climate models (GCMs) and regional climate models to investigate changes in the different parts of the daily precipitation probability density distributions (PDFs), such as the mean or intense/extreme daily precipitation events (Wetherald and Manabe 1999; Kharin and Zwiers 2000; Hegerl et al. 2004; Dai 2006; Kharin et al. 2007; Hegerl et al. 2007; Kiktev et al. 2007; Min et al. 2009;

Seager et al. 2012; Scoccimarro et al. 2013, 2016; Dai et al. 2020; Katiraie-Boroujerdy et al. 2019). These studies found that climate models represent the present-day heavy precipitation in the extratropics reasonably well, but there are also large biases in simulating heavy precipitation in the tropics (e.g., Kharin et al. 2007; O’Gorman and Schneider 2009; Scoccimarro et al. 2013). They showed that future heavy precipitation is generally expected to increase more than the mean precipitation but the large intermodel disagreement in the tropics reduces our confidence on the projections over such domain. In particular, our earlier work (Scoccimarro et al. 2013, hereinafter SCOC13) based on CMIP5 projections demonstrates that the width of the right tail of the precipitation event distribution increases almost everywhere, independently of the direction in which the distribution evolves in a warmer climate; moreover, the regions affected by strong stretching of the right tail of the precipitation event distribution in the future correspond to strong increased availability of water vapor content in the atmospheric column.

The recent availability of a new set of the historical and future climate simulations, performed as part of phase 6 of CMIP (CMIP6; Eyring et al. 2016), makes it

 Denotes content that is immediately available upon publication as open access.

Corresponding author: Enrico Scoccimarro, [enrico.scoccimarro@cmcc.it](mailto:enrico.scoccimarro@cmcc.it)

DOI: 10.1175/JCLI-D-19-0940.1

© 2020 American Meteorological Society. For information regarding reuse of this content and general copyright information, consult the [AMS Copyright Policy](https://www.ametsoc.org/PUBSReuseLicenses) ([www.ametsoc.org/PUBSReuseLicenses](https://www.ametsoc.org/PUBSReuseLicenses)).

TABLE 1. CMIP6 models used in this study. The nominal horizontal grid size is defined following the CMIP6 protocol ([https://pcmdi.github.io/nominal\\_resolution/html/summary.html](https://pcmdi.github.io/nominal_resolution/html/summary.html)).

Model acronym	Extended model name	Nominal horizontal grid size	No. of atmospheric grid points (lat × lon)	Institute (country)	Reference
BCC_CSM2-MR	The Beijing Climate Center Climate System Model 2, Medium Resolution	100 km	160 × 320	Beijing Climate Center (China)	<a href="#">Wu et al. (2019)</a>
CESM2	Community Earth System Model 2	100 km	192 × 288	National Center for Atmospheric Research (United States)	<a href="#">Gettelman et al. (2019)</a>
EC-Earth3-Veg	EC-Earth Consortium model 3–Interactive Vegetation	100 km	256 × 512	European Community Earth System Model (Europe)	<a href="#">EC-Earth (2019)</a>
GFDL-ESM4	Geophysical Fluid Dynamics Laboratory Earth System Model 4	100 km	180 × 288	Geophysical Fluid Dynamics Laboratory (United States)	<a href="#">Guo et al. (2018)</a>
MRI-ESM2.0	Meteorological Research Institute Earth System Model 2.0	100 km	160 × 320	Meteorological Research Institute (Japan)	<a href="#">Yukimoto et al. (2019)</a>
NorESM2-MM	Norwegian Meteorological Institute	100 km	180 × 360	Norwegian Meteorological Institute (Norway)	<a href="#">Øyvind et al. (2020)</a> , manuscript submitted to <i>Geosci. Model Dev.</i>

possible to evaluate the ability of the new generation of GCMs in representing intense and extreme precipitation events over the historical period and to quantify projected changes in the right tail of precipitation probability distributions by the end of the current century. Because horizontal resolution plays an important role in the representation of precipitation patterns in terms of both the mean precipitation and extremes (e.g., [Haarsma et al. 2016](#); [Roberts et al. 2018](#); [Chen and Dai 2019](#)), we may expect a more accurate simulation of the precipitation distribution in time and space by the new CMIP6 models as their resolution and physics represents an improvement over the CMIP5 GCMs.

Within the CMIP6 models, few have a horizontal spacing  $dx$  smaller than 50 km. The High Resolution Model Intercomparison Project (HighResMIP) experiments ([Haarsma et al. 2016](#)) were conducted with grid spacing down to 25 km, but these simulations ended at year 2050. Therefore, currently there are no high-resolution ( $dx \leq 25$  km) future projections to the end of the twenty-first century in the CMIP6 data archive. However, a subset of the CMIP6 models have a nominal  $dx$  of 100 km, which corresponds to the highest resolution available within the CMIP5 models, with simulations under the highest emissions scenario [Shared Socioeconomic Pathway (SSP) SSP5-8.5; [O'Neill et al. 2016](#)]. These models are the ones selected here to investigate their ability in representing intense and extreme daily precipitation at the global scale and to quantify their projected changes in intense daily precipitation under the

highest emissions scenario available from CMIP6. We applied the same method of [SCOC13](#) to evaluate the new CMIP6 models in terms of their ability in simulating the right tail of the daily precipitation PDFs and to quantify their projected changes in heavy daily precipitation events. We also provide additional information on the projected changes in the other parts of the precipitation PDFs, building on additional indices ([Dai et al. 2018](#)) described in [section 2](#).

## 2. Data and methods

### a. Model simulations

We used daily precipitation data from model simulations from the CMIP6 archive ([Eyring et al. 2016](#)). We selected six CMIP6 models ([Table 1](#)) that have a nominal grid spacing of 100 km and provide both historical and SSP5-8.5 future scenario to the end of the current century. [Table 1](#) lists the considered models and summarizes their main characteristics. It is important to say that in the present work the term “CMIP6” just refers to the CMIP6 subsample listed in [Table 1](#).

Three periods are analyzed:

- 1) The period 1996–2014 (labeled VALIDATION), corresponding to the common period between the “historical” CMIP6 simulation and precipitation observations obtained from the Global Precipitation Climatology Project (GPCP; [Bolvin et al. 2009](#)) used for validation.

- 2) The period 1966–2005 (labeled PAST), corresponding to the same 40-yr “historical” baseline used in SCOC13, who analyzed CMIP5 simulations under the RCP8.5 scenario.
- 3) The period 2061–2100 (labeled FUTURE) from the run under the CMIP6 high emissions scenario SSP5-8.5 (O’Neill et al. 2016), the most consistent scenario with the CMIP5 RCP8.5 (Riahi et al. 2011) used in SCOC13.

Both boreal summer [June–August (JJA)] and winter [December–February (DJF)] seasons are considered. The CMIP6 historical simulation was performed with observed concentrations (or emissions, depending on the model implementation) of greenhouse gases, aerosols, ozone, and solar irradiance, starting from an arbitrary point of a quasi-equilibrium control run. The SSP5-8.5 scenario follows a rising radiative forcing pathway leading to  $8.5 \text{ W m}^{-2}$  in 2100.

Model daily precipitation was evaluated using daily precipitation data from the latest version [1 degree daily, version 1.3 (IDD-V1.3)] of the GPCP dataset (Bolvin et al. 2009) on a  $1^\circ$  grid, available from 1996 to 2018. This dataset is obtained by optimally merging estimates computed from microwave, infrared, and sounder data observed by the international constellation of precipitation-related satellites and precipitation gauge analyses. Here we used the GPCP data (hereinafter referred to simply as observations) from 1996 to 2014, which is the end year of the CMIP6 historical simulations. Note that the GPCP’s  $1^\circ$  grid is very close to the nominal grid size of the selected models, making it possible for a direct comparison between them. Otherwise, the high sensitivity of the precipitation PDFs to data resolution would make them incomparable (Chen and Dai 2018). This GPCP dataset has been used previously to quantify precipitation changes (e.g., Liu et al. 2009; Shiu et al. 2012) and evaluate model-simulated intense precipitation (e.g., SCOC13; Scoccimarro et al. 2014, 2016; Villarini et al. 2014).

### b. Methods

We estimated the histograms or frequency distributions of daily precipitation at each grid point using daily precipitation values within DJF or JJA over the 19-yr VALIDATION period for historical simulations and observations. The same was done for the 40-yr PAST and FUTURE periods. We then computed percentiles of the daily precipitation ( $P$ ) time series at each grid point, which included dry days (i.e.,  $P = 0$  cases) in the series, and defined intense (extreme) events as those exceeding the 90th (99th) percentile (denoted as 90p or 99p). The choice to include or not the dry days (all days

or wet days) for the computation of the percentiles for the investigation of extreme precipitation events has been extensively discussed in the literature (e.g., Ban et al. 2015; Schär et al. 2016) and the all-day approach is used here for consistency with SCOC13. To assess how intense precipitation might change in intensity, we examined the future changes in the difference between the 99p and 90p (denoted 99p-90p), as recommended in SCOC13. The 99p-90p metric aims to define the difference in the strength of rainfall associated with intense and extreme precipitation events. This is an additional piece of information, useful to identify regions where there are large differences between the amount of precipitation during extreme and intense events. The proposed metric, thus, is useful to identify potential changes in the right tail of the precipitation distribution, which, in turn, can support impact analyses related to floods: over the regions where heavy precipitation events are clustered in time, an increase of the 99p-90p indicator might lead to an increase in flood risk. This difference metric is defined separately for the VALIDATION, PAST, and FUTURE climates and used to quantify the modeled width of the right tail of the precipitation distribution; it is compared to observations during VALIDATION and its future change is examined. Percentiles are computed for each CMIP6 model at each grid point on its original grid. In addition, we also evaluated the percentage of dry days (the number of days with precipitation  $< 0.1 \text{ mm day}^{-1}$  divided by the total number of days in the period), the frequency of all types of precipitation (with  $P > 1 \text{ mm day}^{-1}$ ), the frequency of light-moderate ( $1 < P \leq 20 \text{ mm day}^{-1}$ ) and heavy precipitation ( $P > 20 \text{ mm day}^{-1}$ ), with the frequency defined as the ratio of the days with such daily precipitation events divided by the total number of days in the period following Dai et al. (2018). The statistics for individual models were then bilinearly interpolated onto the  $1^\circ \times 1^\circ$  grid (same as GPCP) to allow the bias computation at each grid point and the multimodel averaging.

## 3. Results

Despite the increased horizontal resolution in the CMIP6 models, the representation of the right tail of the precipitation distribution appears worse than that in the CMIP5 models (Fig. 1). Compared to observation, there is a large bias in the CMIP6-simulated 99p-90p metric, especially during summer. The worsening of CMIP6 models’ ability in representing the 99p-90p metric (Figs. 1a,b) compared to the CMIP5 models (Figs. 1c,d) is mainly due to changes in the bias of the GFDL model, moving from CMIP5 to CMIP6 version as discussed



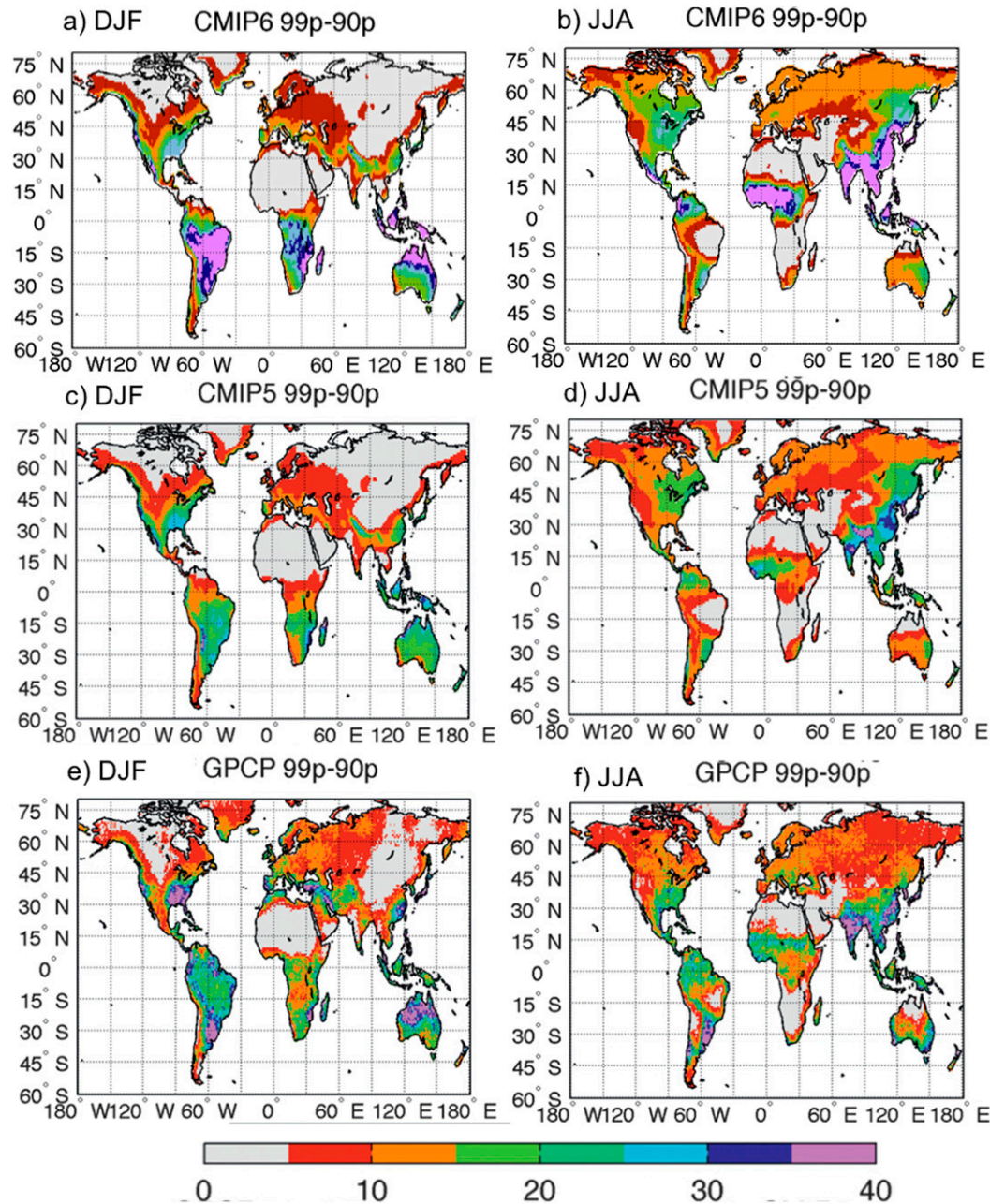


FIG. 1. Measure of the right tail width of the daily precipitation distribution ( $\text{mm day}^{-1}$ ) represented as the difference between the 99th and 90th percentiles of daily precipitation (99p-90p) during the period 1996–2014 obtained from (a),(b) CMIP6, (c),(d) CMIP5 (taken from Fig. 3 in SCOC13), and (e),(f) GPCP observations for (left) DJF and (right) JJA.

below. In the analyzed CMIP6 ensemble, the 90p simulated at mid- and high latitudes is in agreement with observations, but there is a bias of up to  $20 \text{ mm day}^{-1}$  over a significant fraction of the tropical domain, with model-dependent spatial patterns and signs (not shown). The main factor responsible for the positive bias in the 99p-90p metric over the tropics is the large 99p bias,

which is also larger than  $40 \text{ mm day}^{-1}$  for two of the models (BCC\_CSM2-MR and GFDL CM4), over a large fraction of the tropical domain. We verified (not shown) that for the BCC models, the CMIP6 99p positive bias is still large but less pronounced than in its CMIP5 version; and in the GFDL case, over most of the tropics, the CMIP5 bias was negative (but positive in CMIP6),

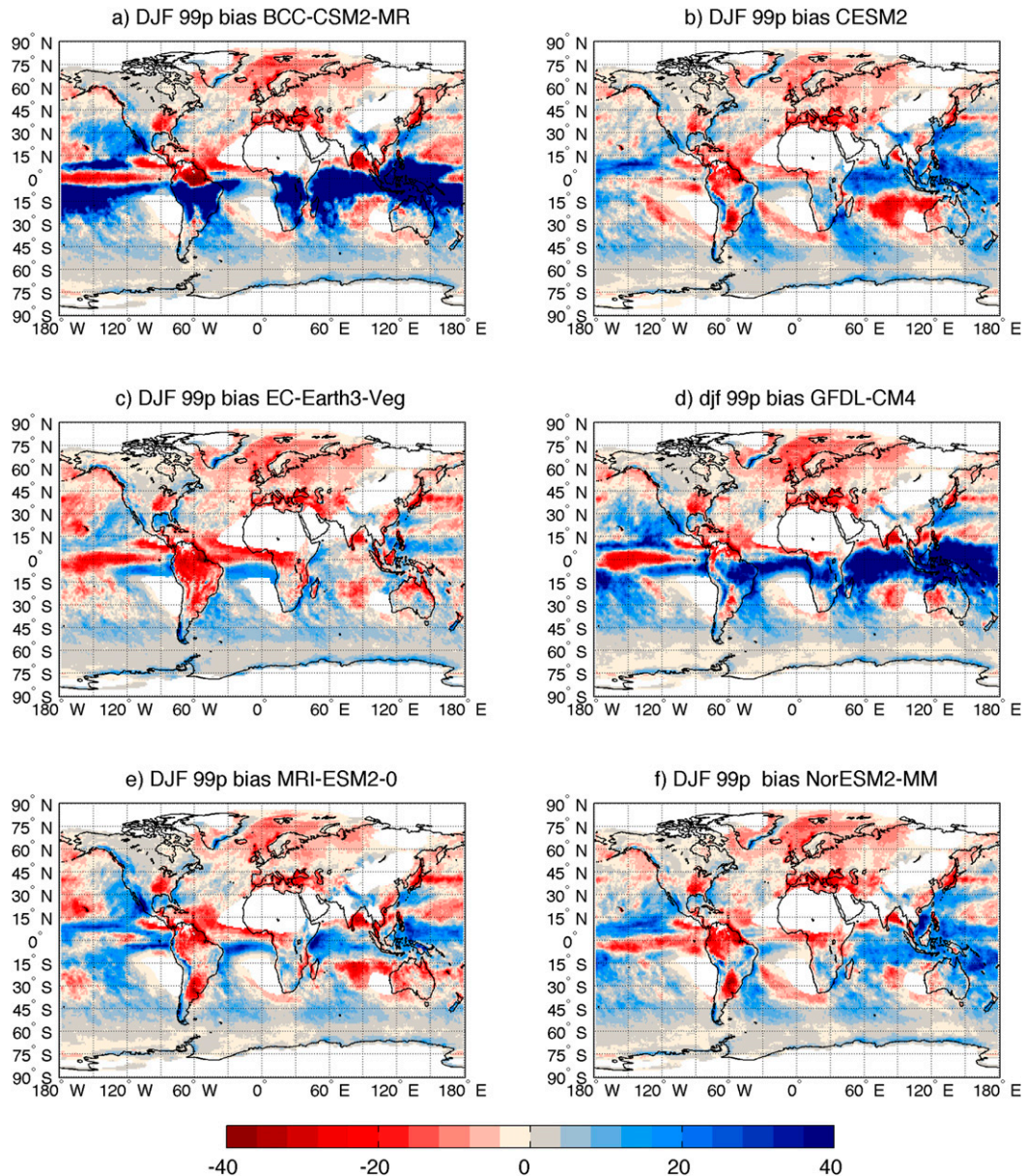


FIG. 2. DJF bias of the 99th percentile of the precipitation ( $\text{mm day}^{-1}$ ) as represented by the considered CMIP6 models under the 1996–2014 period with respect to GPCP observations. White patterns indicate regions with precipitation lower than  $0.5 \text{ mm day}^{-1}$ .

partially compensating the BCC positive bias. The 99p model biases are shown in Fig. 2 for the DJF season, when also a common model tendency to underestimate extreme precipitation is found over the whole Northern Hemisphere and conversely a common model tendency to overestimate extreme precipitation is found over the whole Southern Hemisphere. The opposite tendency is shared by all models during JJA, when a positive and negative bias appears for the whole Northern and Southern Hemisphere, respectively (Fig. 3). Notably,

the aforementioned common CMIP6 models' tendencies at the hemispheric scale are not confirmed by intense (90p) events (not shown). The differences found between CMIP5 and CMIP6 historical results might be related to the different convection scheme applied in their CMIP5 and CMIP6 versions. For instance, the new GFDL model convection scheme is very different from the one adopted in their previous version. In fact, to optimize convection in Atmosphere Model 4.0 (AM4.0), a compromise between the mean state and



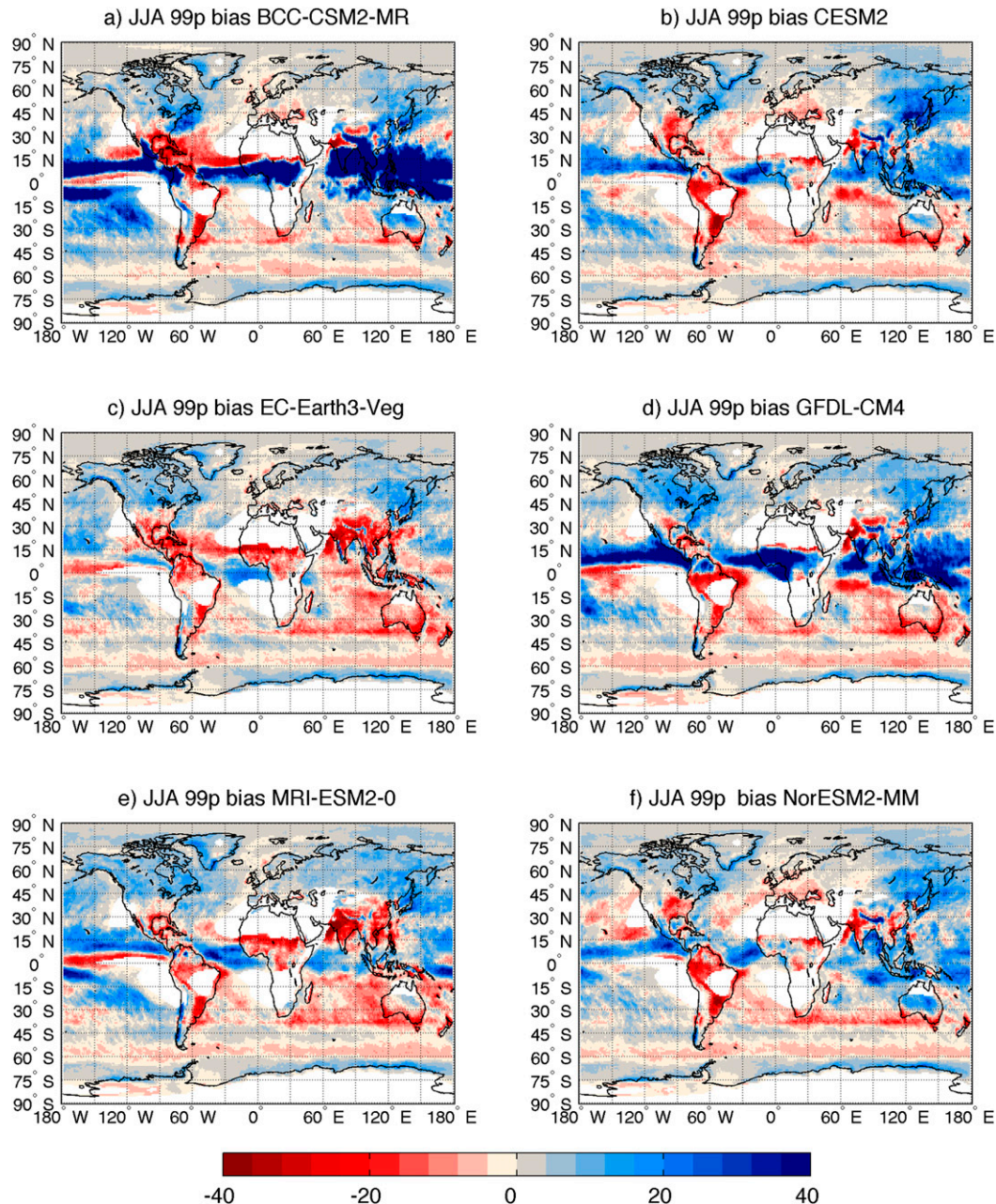


FIG. 3. As in Fig. 2, but for JJA.

tropical transients was considered; the compromise chosen has many realistic features, but also some evident biases such as a tropical upper-tropospheric temperature cold bias and an unrealistic precipitation maximum over some regions. For a discussion of the convection schemes in GFDL CMIP5 and CMIP6 model version the reader is referred to [Zhao et al. \(2018\)](#). Focusing on the BCC model, the CMIP6 version still shows a large positive bias over the tropics despite the slightly lower magnitude for both 90p and 99p, probably

due to the new parameterizations adopted for deep convection and cloud micro/macro physics ([Wu et al. 2019](#)).

The described biases in 90p, 99p, and 99p-90p only partially describe the ability of GCMs in representing the distribution of precipitation events. To extend the model evaluation to the entire precipitation distribution, we verified the CMIP6 models' ability in representing dry days, all type, light-moderate, and heavy precipitation (see methods section): for both DJF and JJA, these biases confirm previous results (e.g., [Dai 2006](#); [Sun et al. 2006](#);

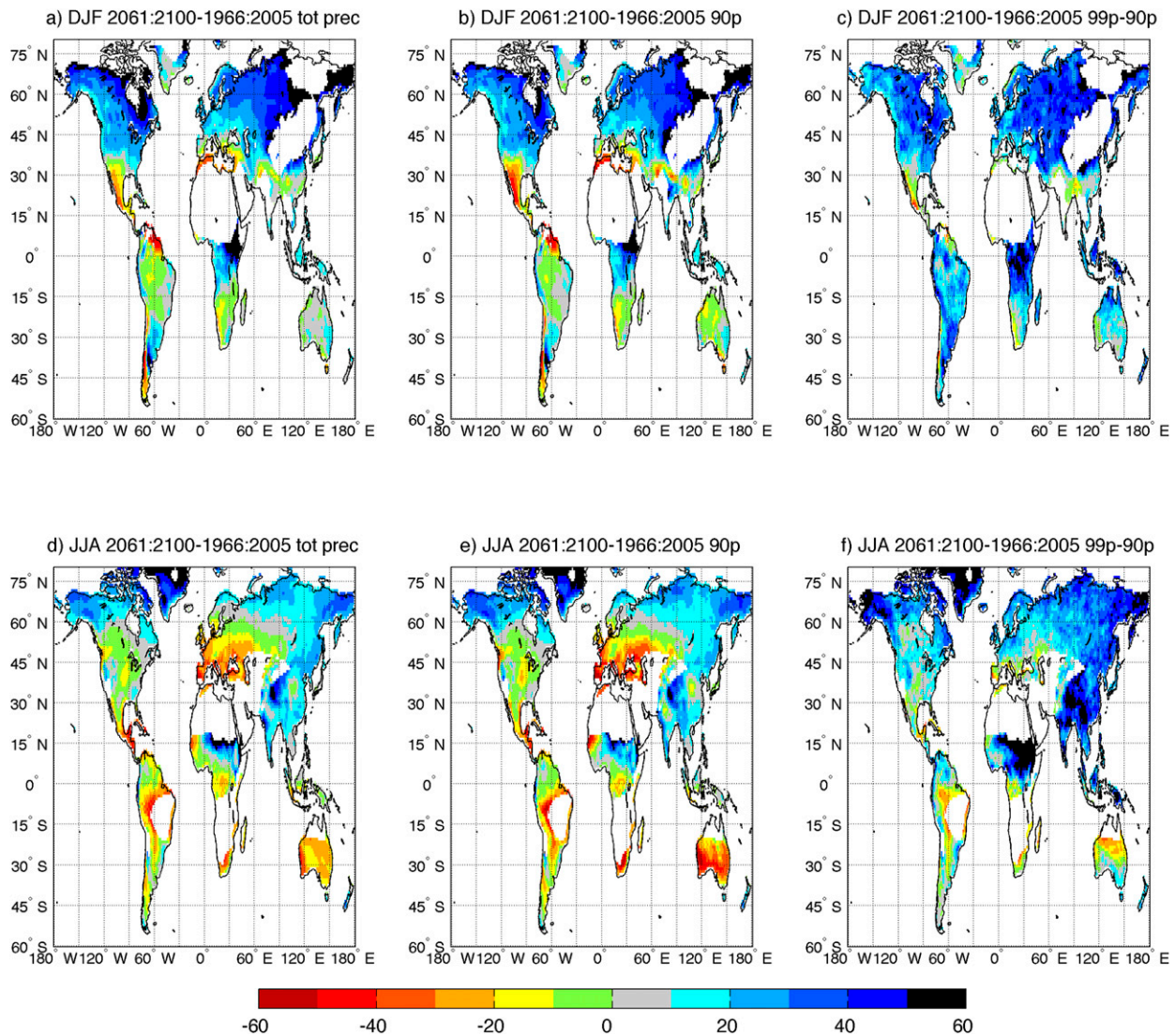


FIG. 4. Future changes (%; 2061–2100 w.r.t. 1966–2005) in (a),(d) total precipitation, (b),(e) 90p, and (c),(f) width of the right tail of the precipitation events' distribution (99p-90p) following the SSP5-8.5 CMIP6 scenario, as averaged over the CMIP6 models for (top) DJF and (bottom) JJA. White patterns over land indicate regions with seasonal precipitation lower than 0.5 mm day<sup>-1</sup>.

Chen and Dai 2019) indicating the general model tendency for too few intense events (when defined based on  $P > 20 \text{ mm day}^{-1}$ ) but too many light-moderate precipitation events. This is not in contrast with the highlighted positive bias in 99p over part of the tropical belt: over certain regions there are few modeled heavy events (i.e., fewer days with precipitation higher than  $20 \text{ mm day}^{-1}$  relative to the observations) but 1% of the events reaching values higher than the observed ones.

In focusing on future projections for the end of the current century, using SSP5-8.5, results are very similar to what emerged in previous CMIP5 models and the RCP8.5. In fact, average, intense (90p), and extreme (99p) events projections (Fig. 4)—expressed in terms of

percentage changes—are comparable to what is shown in Fig. 4 of SCOC13. During boreal winter, there is a general increase in precipitation over land, except for Central and South America, the Mediterranean domain, and northern India. During boreal summer, there is a general increase in precipitation over land at latitudes higher than  $55^\circ\text{N}$ , and a strong decrease over southern Europe, Central America, and part of South America (up to 60%) emerges (red patterns in Fig. 4d). A less intense decrease in total precipitation appears also over western North America, western Africa around  $15^\circ\text{N}$ , the eastern and southern part of South Africa, and most of the Australian domain (Figs. 4a,d). Future changes in 90p (Figs. 4b,e) mainly follow the described changes in



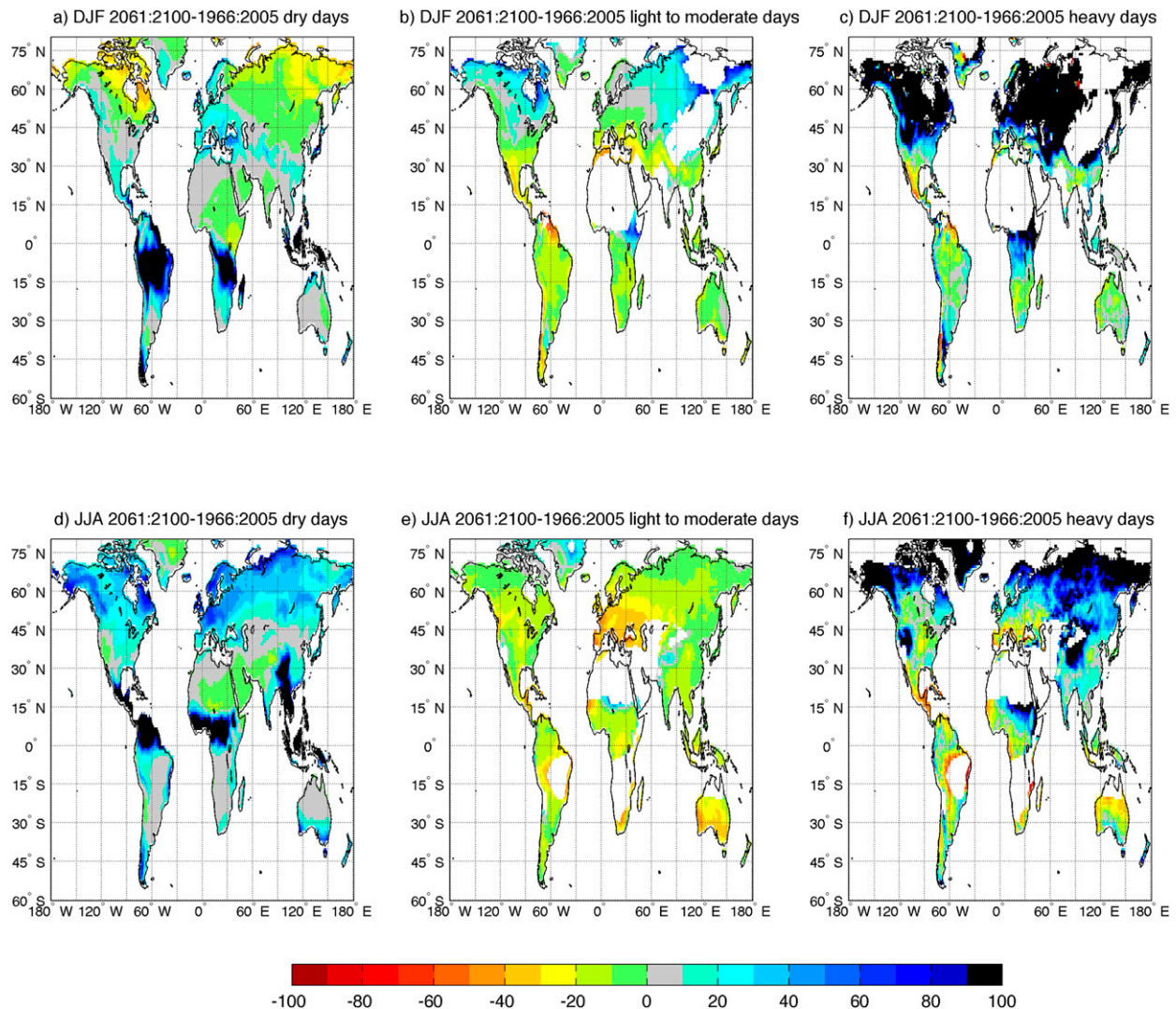


FIG. 5. Future changes (percent change in the fraction of days in the season; 2061–2100 w.r.t. 1966–2005) in (a),(d) dry days ( $P < 0.1 \text{ mm day}^{-1}$ ), (b),(e) light–moderate days ( $1 < P < 20 \text{ mm day}^{-1}$ ), and (c),(f) heavy days ( $P > 20 \text{ mm day}^{-1}$ ) following the SSP5-8.5 CMIP6 scenario, as averaged over the CMIP6 models for (top) DJF and (bottom) JJA. White patterns over land in (b), (c), (e), and (f) indicate regions with seasonal precipitation lower than  $0.5 \text{ mm day}^{-1}$ .

total precipitation, with the exception of a less pronounced percentage increase over most of the domain and a more pronounced decrease over eastern Australia. Projected changes in the right tail of the distribution of precipitation events are shown in terms of the projected 99p-90p metric (Figs. 4c,f) following SCOC13: also in this case future projections are again strongly consistent with CMIP5 results with a global tendency to a stretching of the right tail of the precipitation distribution also over regions where averages and intense events are projected to decrease (red patterns in Fig. 4; e.g., the Euro-Mediterranean domain, especially during boreal summer, and Central America during both seasons). In particular, these results confirmed the case of south-eastern Europe

during boreal summer, where the width of the right tail of the distribution increases, even if the values of nearly the entire precipitation distribution become smaller (i.e., decreases in total and 90p). The most pronounced stretching of the right tail of the precipitation distribution is expected over central Africa between the equator and  $15^{\circ}\text{N}$ , with a projected increase of more than 100% in the FUTURE compared to the PAST period. The projected stretching of the tails of the precipitation distribution over Southern China, Indochina, and the Maritime Continent is less pronounced in CMIP6 SSP5-8.5 than in CMIP5 RCP8.5, but still representative of the most affected regions together with Central Africa.



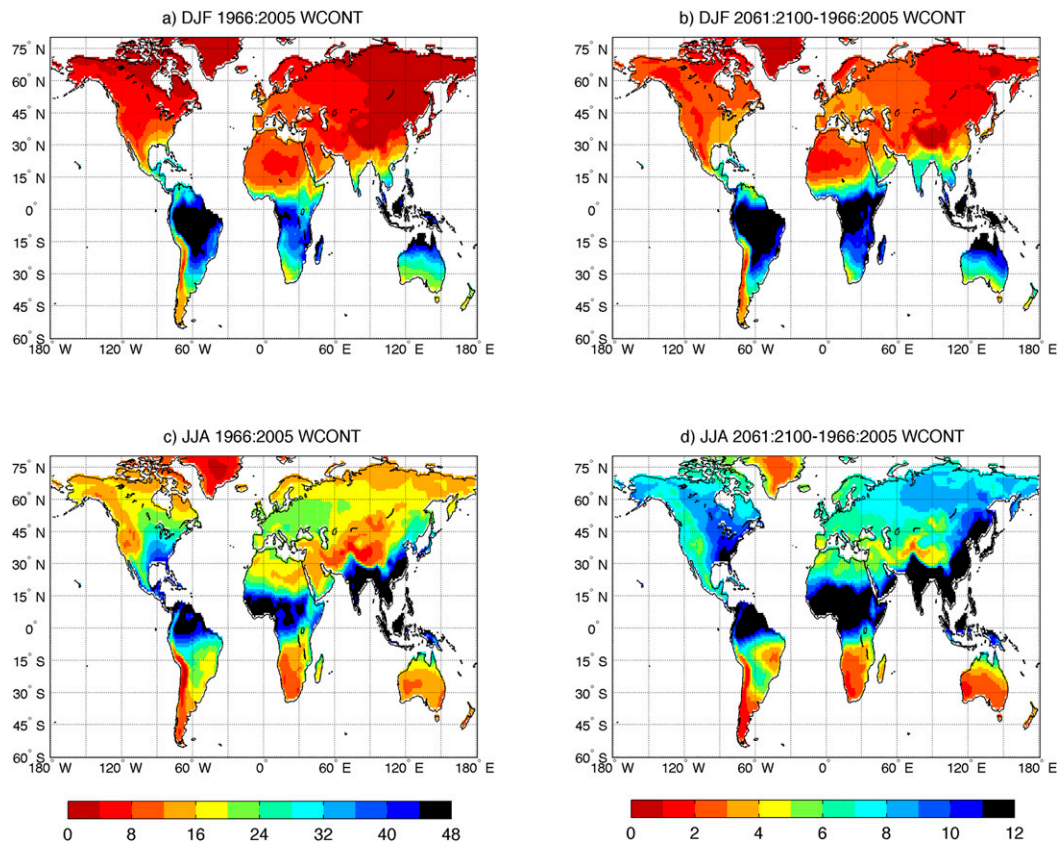


FIG. 6. Vertically integrated water content (WCONT;  $\text{kg m}^{-2}$ ), vertically integrated through the atmospheric column, (a),(c) during the 1966–2005 period and (b),(d) as the increase in 2061–2100 w.r.t. 1966–2005, averaged over the CMIP6 models in (top) DJF and (bottom) JJA.

To better highlight projected changes of the shape of the precipitation distribution, we also considered projections of dry days, light–moderate, and heavy days. CMIP6 projections under the considered scenario confirm previous findings (Dai et al. 2018; Sun et al. 2007): we expect an increase of the extreme precipitation magnitude (already discussed), an increase of the number of heavy days (Figs. 5c,f) and a general tendency to a reduced amount of light–moderate days (Figs. 5b,e). The reduction of light–moderate days is more pronounced during JJA over the European domain (see also Thackeray et al. 2018). Also, the number of dry days is expected to increase over the tropical belt in both DJF and JJA, and to decrease in JJA and increase in DJF north of  $50^{\circ}\text{N}$  (Figs. 5a,d).

#### 4. Discussion and conclusions

It is well known that GCMs are less capable of simulating intense precipitation than high-resolution or convection-permitting regional climate models, but their projected future changes in precipitation distributions

are qualitatively similar (Dai et al. 2020). Here we applied the same approach used by SCOC13 and Dai et al. (2018) to investigate the projected changes in the shape of the daily precipitation distributions in the new CMIP6 models. In particular, we examined the difference between the 99th and 90th percentiles of the daily precipitation simulated by six CMIP6 models with a horizontal grid spacing of  $\sim 100$  km under the SSP5-8.5 scenario to quantify potential changes in the width of the right tail of precipitation distributions.

Mean seasonal precipitation and intense precipitation (the 90th percentile) are simulated reasonably well in both CMIP5 (SCOC13) and CMIP6 models. However, two of the six CMIP6 models greatly overestimate the 99th percentile of the precipitation distribution, leading an overestimation of the 99p–90p difference metric, especially in the tropics. Based on recent findings on the link between tropical extreme precipitation and extratropical events (Boers et al. 2019), a degradation of a GCM’s ability in representing tropical extreme precipitation could also affect its ability to simulate such events over the extratropical domain. This highlights

the importance of improved precipitation parameterization, in addition to increased horizontal resolution.

Consistent with the CMIP5 results, CMIP6 projections suggest that daily precipitation intensity tends to increase more than mean precipitation over most land areas under a warmer climate, confirming previous findings (e.g., Trenberth et al. 2003; Meehl et al. 2005; Chou et al. 2009; Pall et al. 2007; O’Gorman and Schneider 2009; SCOC13; Toreti et al. 2013; Scoccimarro et al. 2014; Trenberth et al. 2015; Zhang et al. 2017; Carmichael et al. 2018; Sonkoué et al. 2019). This is also consistent with a higher capacity of the warmer air to hold moisture contributing to greater moisture convergence (e.g., Trenberth et al. 2003; Tebaldi et al. 2006) and with the Clausius–Clapeyron dependence, relevant for heavy precipitation events (Held and Soden 2006; Scoccimarro et al. 2015). Thus, the shift toward heavier precipitation already shown by previous models (Sun et al. 2007; SCOC13; Dai et al. 2018) is also confirmed by the last-generation CMIP6 experiments. Confirming SCOC13, the width of the right tail of daily precipitation distributions increases almost everywhere (Fig. 4), independent of the direction in which the distribution evolves in the SSP5-8.5 warmer climate. We know that projected changes of extreme precipitation are driven both by dynamic (mass convergence) and thermodynamic (moisture content) tendencies (e.g., Pfahl et al. 2017; Norris et al. 2019; Chen et al. 2019). Focusing on the thermodynamic component, the regions affected by large stretching of the right tail of the daily precipitation distributions in the future (blue patterns in Fig. 4) correspond to large increases in atmospheric water vapor content (blue patterns in Figs. 6b,d). This is consistent with the CMIP5 results (SCOC13).

*Acknowledgments.* We gratefully acknowledge the support of the EU project COACCH Grant Agreement 776479 for help in providing data and tools for the extreme event analysis. The comments by the editor and two anonymous reviewers are gratefully acknowledged.

## REFERENCES

- Ban, N., J. Schmidli, and C. Schär, 2015: Heavy precipitation in a changing climate: Does short-term summer precipitation increase faster? *Geophys. Res. Lett.*, **42**, 1165–1172, <https://doi.org/10.1002/2014GL062588>.
- Boers, N., B. Goswami, A. Rheinwalt, B. Bookhagen, B. Hoskins, and J. Kurths, 2019: Complex networks reveal global pattern of extreme-rainfall teleconnections. *Nature*, **566**, 373–377, <https://doi.org/10.1038/s41586-018-0872-x>.
- Bolvin, D. T., R. F. Adler, G. J. Huffman, E. J. Nelkin, and J. P. Poutiainen, 2009: Comparison of GPCP monthly and daily precipitation estimates with high-latitude gauge observations. *J. Appl. Meteor. Climatol.*, **48**, 1843–1857, <https://doi.org/10.1175/2009JAMC2147.1>.
- Carmichael, M. J., R. D. Pancost, and D. J. Lunt, 2018: Changes in the occurrence of extreme precipitation events at the Paleocene–Eocene thermal maximum. *Earth Planet. Sci. Lett.*, **501**, 24–36, <https://doi.org/10.1016/j.epsl.2018.08.005>.
- Chen, D., and A. Dai, 2018: Dependence of estimated precipitation frequency and intensity on data resolution. *Climate Dyn.*, **50**, 3625–3647, <https://doi.org/10.1007/s00382-017-3830-7>.
- , and —, 2019: Precipitation characteristics in the Community Atmosphere Model and their dependence on model physics and resolution. *J. Adv. Model. Earth Syst.*, **11**, 2352–2374, <https://doi.org/10.1029/2018MS001536>.
- Chen, G., J. Norris, J. D. Neelin, J. Lu, L. R. Leung, and K. Sakaguchi, 2019: Thermodynamic and dynamic mechanisms for hydrological cycle intensification over the full probability distribution of precipitation events. *J. Atmos. Sci.*, **76**, 497–516, <https://doi.org/10.1175/JAS-D-18-0067.1>.
- Chou, C., J. D. Neelin, C. Chen, and J. Tu, 2009: Evaluating the “rich-get-richer” mechanism in tropical precipitation change under global warming. *J. Climate*, **22**, 1982–2005, <https://doi.org/10.1175/2008JCLI2471.1>.
- Dai, A., 2006: Precipitation characteristics in eighteen coupled climate models. *J. Climate*, **19**, 4605–4630, <https://doi.org/10.1175/JCLI3884.1>.
- , T. Zhao, and J. Chen, 2018: Climate change and drought: A precipitation and evaporation perspective. *Curr. Climate Change Rep.*, **4**, 301–312, <https://doi.org/10.1007/s40641-018-0101-6>.
- , R. M. Rasmussen, C. Liu, K. Ikeda, and A. F. Prein, 2020: A new mechanism for warm-season precipitation response to global warming based on convection-permitting simulations. *Climate Dyn.*, **55**, 343–368, <https://doi.org/10.1007/s00382-017-3787-6>.
- EC-Earth, 2019: EC-Earth-Consortium EC-Earth3-veg model output prepared for CMIP6 ScenarioMIP. Earth System Grid Federation, accessed 25 February 2020, <https://doi.org/10.22033/ESGF/CMIP6.727>.
- Eyring, V., S. Bony, G. A. Meehl, C. Senior, B. Stevens, R. J. Stouffer, and K. E. Taylor, 2016: Overview of the Coupled Model Intercomparison Project Phase 6 (CMIP6) experimental design and organisation. *Geosci. Model Dev. Discuss.*, **8**, 10 539–10 583, <https://doi.org/10.5194/gmd-8-10539-2015>.
- Gettelman, A., and Coauthors, 2019: High climate sensitivity in the Community Earth System Model version 2 (CESM2). *Geophys. Res. Lett.*, **46**, 8329–8337, <https://doi.org/10.1029/2019GL083978>.
- Guo, H., and Coauthors, 2018: NOAA-GFDL GFDL-CM4 model output. Earth System Grid Federation, accessed 1 July 2018, <https://doi.org/10.22033/ESGF/CMIP6.1402>.
- Haarsma, R. J., and Coauthors, 2016: High Resolution Model Intercomparison Project (HighResMIP). *Geosci. Model Dev.*, **9**, 4185–4208, <https://doi.org/10.5194/gmd-9-4185-2016>.
- Hegerl, G. C., F. W. Zwiers, P. A. Stott, and V. V. Kharin, 2004: Detectability of anthropogenic changes in annual temperature and precipitation extremes. *J. Climate*, **17**, 3683–3700, [https://doi.org/10.1175/1520-0442\(2004\)017<3683:DOACIA>2.0.CO;2](https://doi.org/10.1175/1520-0442(2004)017<3683:DOACIA>2.0.CO;2).
- , and Coauthors, 2007: Understanding and attributing climate change. *Climate Change 2007: The Physical Science Basis*, S. Solomon et al., Eds., Cambridge University Press, 663–745.
- Held, I. M., and B. J. Soden, 2006: Robust responses of the hydrological cycle to global warming. *J. Climate*, **19**, 5686–5699, <https://doi.org/10.1175/JCLI3990.1>.
- Katiraie-Boroujerdy, P. S., A. A. Asanjan, A. Chavoshian, K. Hsu, and S. Sorooshian, 2019: Assessment of seven CMIP5 model



- precipitation extremes over Iran based on a satellite-based climate data set. *Int. J. Climatol.*, **39**, 3505–3522, <https://doi.org/10.1002/joc.6035>.
- Kharin, V. V., and F. W. Zwiers, 2000: Changes in the extremes in an ensemble of transient climate simulations with a coupled atmosphere–ocean GCM. *J. Climate*, **13**, 3760–3788, [https://doi.org/10.1175/1520-0442\(2000\)013<3760:CITEIA>2.0.CO;2](https://doi.org/10.1175/1520-0442(2000)013<3760:CITEIA>2.0.CO;2).
- , —, X. Zhang, and G. C. Hegerl, 2007: Changes in temperature and precipitation extremes in the IPCC ensemble of global coupled model simulations. *J. Climate*, **20**, 1419–1444, <https://doi.org/10.1175/JCLI4066.1>.
- Kiktev, D., J. Caesar, L. V. Alexander, H. Shiogama, and M. Collier, 2007: Comparison of observed and multimodeled trends in annual extremes of temperature and precipitation. *Geophys. Res. Lett.*, **34**, L10702, <https://doi.org/10.1029/2007GL029539>.
- Liu, S. C., C. Fu, C.-J. Shiu, J.-P. Chen, and F. Wu, 2009: Temperature dependence of global precipitation extremes. *Geophys. Res. Lett.*, **36**, L17702, <https://doi.org/10.1029/2009GL040218>.
- Meehl, G. A., and S. Bony, 2012: Introduction to CMIP5. *CLIVAR Exchanges*, No. 56, International CLIVAR Project Office, Southampton, United Kingdom, 4–5 <http://www.clivar.org/sites/default/files/documents/Exchanges56.pdf>.
- , J. M. Arblaster, and C. Tebaldi, 2005: Understanding future patterns of increased precipitation intensity in climate model simulations. *Geophys. Res. Lett.*, **32**, L18719, <https://doi.org/10.1029/2005GL023680>.
- , C. Covey, T. Delworth, M. Latif, B. McAvaney, J. F. B. Mitchell, R. J. Stouffer, and K. E. Taylor, 2007: The WCRP CMIP3 multimodel dataset: A new era in climate change research. *Bull. Amer. Meteor. Soc.*, **88**, 1383–1394, <https://doi.org/10.1175/BAMS-88-9-1383>.
- Min, S.-K., X. B. Zhang, F. W. Zwiers, P. Friederichs, and A. Hense, 2009: Signal detectability in extreme precipitation changes assessed from twentieth century climate simulations. *Climate Dyn.*, **32**, 95–111, <https://doi.org/10.1007/s00382-008-0376-8>.
- Norris, J., G. Chen, and J. D. Neelin, 2019: Thermodynamic versus dynamic controls on extreme precipitation in a warming climate from the Community Earth System Model Large Ensemble. *J. Climate*, **32**, 1025–1045, <https://doi.org/10.1175/JCLI-D-18-0302.1>.
- O’Gorman, P. A., and T. Schneider, 2009: The physical basis for increases in precipitation extremes in simulations of 21st-century climate change. *Proc. Natl. Acad. Sci. USA*, **106**, 14 773–14 777, <https://doi.org/10.1073/pnas.0907610106>.
- O’Neill, B. C., and Coauthors, 2016: The Scenario Model Intercomparison Project (ScenarioMIP) for CMIP6. *Geosci. Model Dev.*, **9**, 3461–3482, <https://doi.org/10.5194/gmd-9-3461-2016>.
- Pall, P., M. R. Allen, and D. A. Stone, 2007: Testing the Clausius–Clapeyron constraint on changes in extreme precipitation under CO<sub>2</sub> warming. *Climate Dyn.*, **28**, 351–363, <https://doi.org/10.1007/s00382-006-0180-2>.
- Pfahl, S., P. A. O’Gorman, and E. M. Fischer, 2017: Understanding the regional pattern of projected future changes in extreme precipitation. *Nat. Climate Change*, **7**, 423–427, <https://doi.org/10.1038/nclimate3287>.
- Riahi, K., and Coauthors, 2011: RCP 8.5—A scenario of comparatively high greenhouse gas emissions. *Climatic Change*, **109**, 33–57, <https://doi.org/10.1007/s10584-011-0149-y>.
- Roberts, M., and Coauthors, 2018: The benefits of global high resolution for climate simulation: Process-understanding and the enabling of stakeholder decisions at the regional scale. *Bull. Amer. Meteor. Soc.*, **99**, 2341–2359, <https://doi.org/10.1175/BAMS-D-15-00320.1>.
- Schär, C., and Coauthors, 2016: Percentile indices for assessing changes in heavy precipitation events. *Climatic Change*, **137**, 201–216, <https://doi.org/10.1007/s10584-016-1669-2>.
- Scoccimarro, E., S. Gualdi, A. Bellucci, M. Zampieri, and A. Navarra, 2013: Heavy precipitation events in a warmer climate: Results from CMIP5 models. *J. Climate*, **26**, 7902–7911, <https://doi.org/10.1175/JCLI-D-12-00850.1>.
- , —, G. Villarini, G. Vecchi, M. Zhao, K. Walsh, and A. Navarra, 2014: Intense precipitation events associated with landfalling tropical cyclones in response to a warmer climate and increased CO<sub>2</sub>. *J. Climate*, **27**, 4642–4654, <https://doi.org/10.1175/JCLI-D-14-00065.1>.
- , G. Villarini, M. Vichi, M. Zampieri, P. G. Fogli, A. Bellucci, and S. Gualdi, 2015: Projected changes in intense precipitation over Europe at the daily and sub-daily time scales. *J. Climate*, **28**, 6193–6203, <https://doi.org/10.1175/JCLI-D-14-00779.1>.
- , S. Gualdi, A. Bellucci, M. Zampieri, and A. Navarra, 2016: Heavy precipitation events over the Euro-Mediterranean region in a warmer climate: Results from CMIP5 models. *Reg. Environ. Change*, **16**, 595–602, <https://doi.org/10.1007/s10113-014-0712-y>.
- Seager, R., N. Naik, and L. Vogel, 2012: Does global warming cause intensified interannual hydroclimate variability? *J. Climate*, **25**, 3355–3372, <https://doi.org/10.1175/JCLI-D-11-00363.1>.
- Shiu, C.-J., S. C. Liu, C. Fu, A. Dai, and Y. Sun, 2012: How much do precipitation extremes change in a warming climate? *Geophys. Res. Lett.*, **39**, L17707, <https://doi.org/10.1029/2012GL052762>.
- Sonkoué, D., D. Monkam, T. C. Fotso-Nguemo, Z. D. Yepdo, and D. A. Vondou, 2019: Evaluation and projected changes in daily rainfall characteristics over central Africa based on a multi-model ensemble mean of CMIP5 simulations. *Theor. Appl. Climatol.*, **137**, 2167–2186, <https://doi.org/10.1007/s00704-018-2729-5>.
- Sun, Y., S. Solomon, A. Dai, and R. Portmann, 2006: How often does it rain? *J. Climate*, **19**, 916–934, <https://doi.org/10.1175/JCLI3672.1>.
- , —, —, and —, 2007: How often will it rain? *J. Climate*, **20**, 4801–4818, <https://doi.org/10.1175/JCLI4263.1>.
- Taylor, K. E., R. J. Stouffer, and G. A. Meehl, 2012: An overview of CMIP5 and the experiment design. *Bull. Amer. Meteor. Soc.*, **93**, 485–498, <https://doi.org/10.1175/BAMS-D-11-00094.1>.
- Tebaldi, C., K. Hayhoe, J. M. Arblaster, and G. A. Meehl, 2006: Going to the extremes: An intercomparison of model-simulated historical and future changes in extreme events. *Climatic Change*, **79**, 185–211, <https://doi.org/10.1007/s10584-006-9051-4>.
- Thackeray, C. W., A. M. DeAngelis, A. Hall, D. L. Swain, and X. Qu, 2018: On the connection between global hydrologic sensitivity and regional wet extremes. *Geophys. Res. Lett.*, **45**, 11–343, <https://doi.org/10.1029/2018GL079698>.
- Toreti, A., and Coauthors, 2013: Projections of global changes in precipitation extremes from Coupled Model Intercomparison Project phase 5 models. *Geophys. Res. Lett.*, **40**, 4887–4892, <https://doi.org/10.1002/grl.50940>.
- Trenberth, K. E., A. Dai, R. Rasmussen, and D. Parsons, 2003: The changing character of precipitation. *Bull. Amer. Meteor. Soc.*, **84**, 1205–1218, <https://doi.org/10.1175/BAMS-84-9-1205>.
- , J. T. Fasullo, and T. G. Shepherd, 2015: Attribution of climate extreme events. *Nat. Climate Change*, **5**, 725–730, <https://doi.org/10.1038/nclimate2657>.

- Villarini, G., D. A. Lavers, E. Scoccimarro, M. Zhao, M. F. Wehner, G. Vecchi, and T. Knutson, 2014: Sensitivity of tropical cyclone rainfall to idealized global scale forcings. *J. Climate*, **27**, 4622–4641, <https://doi.org/10.1175/JCLI-D-13-00780.1>.
- Wetherald, R. T., and S. Manabe, 1999: Detectability of summer dryness caused by greenhouse warming. *Climatic Change*, **43**, 495–511, <https://doi.org/10.1023/A:1005499220385>.
- Wu, T., and Coauthors, 2019: The Beijing Climate Center Climate System Model (BCC-CSM): The main progress from CMIP5 to CMIP6. *Geosci. Model Dev.*, **12**, 1573–1600, <https://doi.org/10.5194/gmd-12-1573-2019>.
- Yukimoto, S., and Coauthors, 2019: MRI MRI-ESM2.0 model output prepared for CMIP6 CMIP. Earth System Grid Federation, accessed 8 November 2019, <https://doi.org/10.22033/ESGF/CMIP6.621>.
- Zhang, W., G. Villarini, E. Scoccimarro, and G. Vecchi, 2017: Stronger influences of increased CO<sub>2</sub> on subdaily precipitation extremes than at the daily scale. *Geophys. Res. Lett.*, **44**, 7464–7471, <https://doi.org/10.1002/2017GL074024>.
- Zhao, M., and Coauthors, 2018: The GFDL Global Atmosphere and Land Model AM4.0/LM4.0: 2. Model description, sensitivity studies, and tuning strategies. *J. Adv. Model. Earth Syst.*, **10**, 735–769, <https://doi.org/10.1002/2017MS001209>.